*J Mater Sci* (2018) 53:13912–13923

Chemical routes to materials

# Synergistically enhanced peroxidase-like activity of Pd nanoparticles dispersed on $CeO_2$ nanotubes and their application in colorimetric sensing of sulfhydryl compounds

Xin Li[1], Zhilong Pu[1], Hao Zhou[1], Wenchi Zhang[1], Xiangheng Niu[1,2,*], Yanfang He[1], Xuechao Xu[3], Fengxian Qiu[1,*], Jianming Pan[1,2], and Liang Ni[1,*]

[1] School of Chemistry and Chemical Engineering, Jiangsu University, Zhenjiang 212013, China
[2] Institute of Green Chemistry and Chemical Technology, Jiangsu University, Zhenjiang 212013, China
[3] School of Food and Biological Engineering, Jiangsu University, Zhenjiang 212013, China

**Received:** 14 April 2018
**Accepted:** 27 June 2018
**Published online:** 2 July 2018



## ABSTRACT

In this work, we proposed a new hybrid of Pd nanoparticles dispersed on $CeO_2$ nanotubes (Pd NPs/$CeO_2$ NTs) with synergistically enhanced peroxidase-like activity for the visual detection of sulfhydryl compounds. In comparison with individual Pd NPs and $CeO_2$ NTs, the Pd NPs/$CeO_2$ NTs hybrid exhibited a synergy effect to trigger the oxidation of colorless 3,3′,5,5′-tetramethylbenzidine (TMB) to its blue product TMBox mediated by $H_2O_2$. It was further demonstrated that the improved activity observed in Pd NPs/$CeO_2$ NTs originated from the strong interplays between Pd NPs and $CeO_2$ NTs, which could significantly increase the $Ce^{3+}/Ce^{4+}$ ratio. Besides, sulfhydryl compounds were found to have the capacity to suppress the color reaction of TMB + $H_2O_2$ catalyzed by the Pd NPs/$CeO_2$ NTs nanozyme at a low level. Based on this principle, mercaptoacetic acid in the concentration range of 66–400 nM could be linearly determined. Similarly, sulfhydryl-containing amino acid (cysteine) and its derivative (glutathione) in the linear scope of 6–40 nM were also detected, providing a detection limit down to 2.9 and 11.3 nM, respectively.

## Introduction

In the past decade, nanomaterials with enzyme-like characteristics (nanozymes) have been drawing growing interest of scientists thanks to their merits of easy mass production, low cost, and excellent robustness against harsh environments [1–6]. These advantages have endowed them with extensive applications in chemo- and biosensing [7–21]. Nevertheless, compared with natural bio-enzymes and organic catalysts, the catalytic activities and

Address correspondence to E-mail: niuxiangheng@126.com; fxqiu@ujs.edu.cn; niliang@ujs.edu.cn


https://doi.org/10.1007/s10853-018-2657-x

efficiencies of most nanozymes developed are still lower, which inevitably impede their wider applications. Therefore, exploiting nanozymes with desired activities and efficiencies for chemo- and biosensing turns to be of great importance [1].

Up to now, several strategies have been proposed to improve the catalytic activities and efficiencies of nanozymes, including tailoring shape [22], controlling size [23], optimizing composition [24], adjusting crystal facet [25], modifying surface [26, 27], and forming hybrids [28–32]. Among these approaches, fabricating nanozyme hybrids is particularly impressive, because it is able to combine the respective features of each component together and even to achieve cooperatively enhanced properties. For example, Zhao and co-workers [30] dispersed $CeO_2$ particles onto $TiO_2$ nanotubes ($CeO_2$/NT-$TiO_2$) and observed a higher peroxidase-like activity in the formed hybrid compared with the $CeO_2$ counterpart. Qu's group reported a GO-AuNCs hybrid that could exhibit excellent peroxidase-like activity at neutral pH, whereas both GO and AuNCs showed almost no activity under the same condition [33]. These attractive results inspire us to exploit novel nanozyme hybrids with favorable performance for their promising applications in biochemical analysis. As a common rare-earth metal oxide, $CeO_2$ is a promising peroxidase mimic. The mixed valence of Ce in the oxide exhibits a strong redox behavior, and the $Ce^{4+}$/$Ce^{3+}$ redox couple can switch to each other through the $CeO_2 \leftrightarrow CeO_{2-x} + x/2O_2$ ($Ce^{4+} \leftrightarrow Ce^{3+}$) process, which is similar to natural redox enzymes. The noble metal Pd is widely used in various fields because of its good catalytic activity. It has been reported that both Pd and $CeO_2$ nanoparticles can be used as nanozymes. Singh et al. [34] developed a Pd-Au bimetallic peroxidase-like nanozyme for colorimetric sensing of malathion. $CeO_2$ also shows mimetic properties of multi-enzymes including peroxidase [35, 36]. Therefore, combining the two nanozymes together to form a hybrid may bring some new enzymatic properties.

In this work, we reported a new hybrid of $CeO_2$ nanotube-supported Pd nanoparticles (Pd NPs/$CeO_2$ NTs) with significantly enhanced peroxidase-like activity for the colorimetric sensing of sulfhydryl compounds. The synthesized Pd NPs/$CeO_2$ NTs hybrid could provide a synergy effect to catalyze the oxidation of 3,3′,5,5′-tetramethylbenzidine (TMB) in the presence of $H_2O_2$. The enzymatic properties of the proposed Pd NPs/$CeO_2$ NTs were systematically investigated, and the underlying mechanism for its improved activity was elucidated. Furthermore, sulfhydryl compounds were found to suppress the color reaction via reducing the catalytic activity of the peroxidase mimic and/or competitively reacting with generated hydroxyl radicals against TMB. With this principle, sulfhydryl-containing species including mercaptoacetic acid, cysteine, and glutathione could be determined with good performance.

## Materials and methods

### Chemicals

$Ce(NO_3)_3{\cdot}6H_2O$, $NH_3{\cdot}H_2O$, $PdCl_2$, $NaBH_4$, $H_2O_2$, TMB, and mercaptoacetic acid were purchased from Sinopharm Chemical Reagent Co., Ltd. Cysteine (Cys) and glutathione (GSH) were provided by Shanghai Aladdin Biochemical Technology Co., Ltd. Deionized water was utilized throughout the study. All other chemicals were of analytical grade and directly used without further purification.

### Synthesis of Pd NPs/$CeO_2$ NTs

The preparation of Pd NPs/$CeO_2$ NTs was performed according to Scheme 1. Typically, 4.3397 g $Ce(NO_3)_3{\cdot}6H_2O$ was first dissolved into 100 mL deionized water; a certain amount of $NH_3{\cdot}H_2O$ was then added into the solution till pH 9 to form $Ce(OH)_4$; afterward, the collected $Ce(OH)_4$ product was calcinated in air (a heating rate of 2 °C $min^{-1}$, calcinated at 550 °C for 5 h) to generate $CeO_2$ NTs, and the yield of the $CeO_2$ NTs product was 0.5819 g. 0.0430 g $CeO_2$ NTs and 5 mL of 25 mM $PdCl_2$ precursor solution were mixed in 20 mL deionized water with a mild stir for 30 min; 10 mL of 50 mM $NaBH_4$ solution was then dropped into the suspension for reaction for another 30 min; afterward, the formed Pd NPs/$CeO_2$ NTs hybrid was washed with adequate deionized water and collected by centrifugation. For comparison, individual Pd NPs and $CeO_2$ NTs were also prepared with similar procedures.

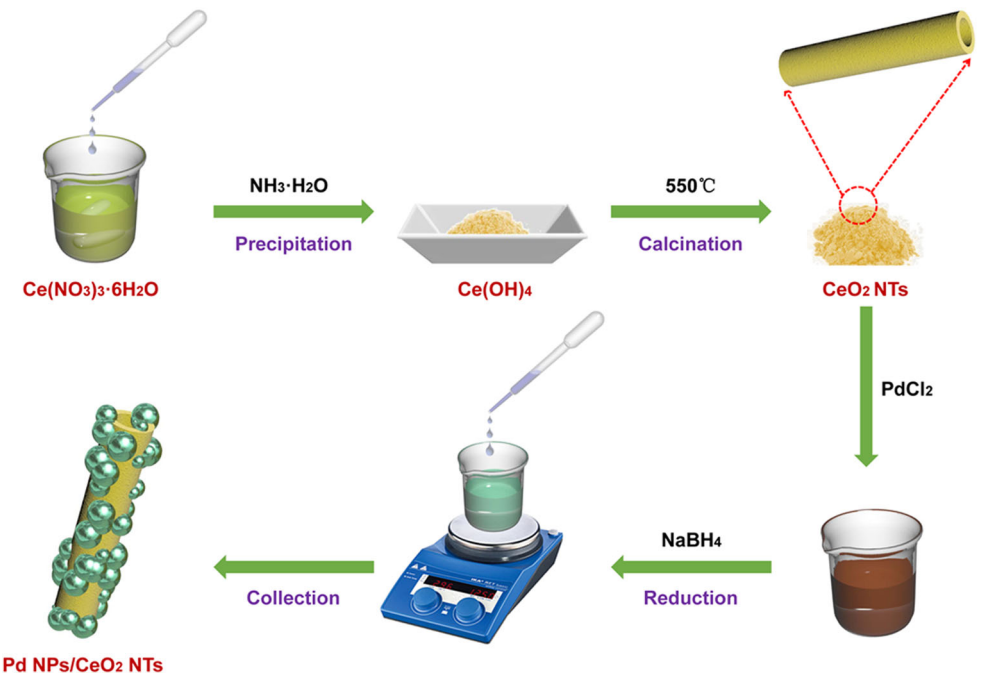


**Scheme 1** Illustration for the synthesis of Pd NPs/$CeO_2$ NTs.

## Characterization

The crystal phase of synthesized materials was analyzed by an X-ray diffractometer (XRD, 6100Lab, Rigaku Co., Ltd.) with a Cu Kα source ($\lambda$ = 0.154056 nm, 40 kV, 30 mA). Transmission electron microscopy (TEM) images were captured on a JEM-2100 microscope (JEOL). An IRIS-1000 inductively coupled plasma optical emission spectroscope (ICP-OES, Thermo-Fisher Scientific Co., Ltd.) was used to precisely determine the concentration of Pd NPs/$CeO_2$ NTs. The surface chemistry of peroxidase mimics was studied by an X-ray photoelectron spectrometer (XPS, ESCALAB 250Xi, Thermo-Fisher Scientific Co., Ltd.).

## Colorimetric measurements

The peroxidase-like activities of synthesized materials were investigated by the catalytic oxidation of TMB in the presence of $H_2O_2$. All the reactions were measured by a UV-2450 ultraviolet–visible (UV–Vis) spectrometer (Shimadzu). A 5 mM TMB stock solution was prepared with ethanol for use. $H_2O_2$ stock solutions with various concentrations were freshly prepared. 0.2 M NaAc–HAc solutions with different pH values (adjusted by diluted HCl or NaOH) were prepared as the incubation buffer. Typically, colorimetric measurements were performed in a 5-mL quartz cell with 3-mL NaAc–HAc buffer (0.2 M, pH 4.0) containing 1.67 μg $mL^{-1}$ nanozyme, 0.327 M $H_2O_2$, and 0.167 mM TMB. The time-dependent absorbance changes were recorded with a 30-s interval.

Steady-state kinetic measurements were carried out by recording the absorbance at 652 nm at a 5-s interval within 1.5 min. In each group, only the concentration of $H_2O_2$ or TMB varied at a time, and other conditions remained fixed. The apparent kinetic parameters were calculated based on the equation $\upsilon = V_{max} \times [S]/(K_m + [S])$, where $\upsilon$ is the initial velocity, $V_{max}$ is the maximum reaction velocity, $[S]$ is the substrate ($H_2O_2$ or TMB) concentration, and $K_m$ is the Michaelis–Menten constant. In addition, the catalytic constant $k_{cat}$ was calculated based on the equation $k_{cat} = V_{max}/[E]$, where $[E]$ is the concentration of the enzyme used.

For the detection of mercaptoacetic acid, Cys, or GSH, 2.6-mL NaAc–HAc buffer (0.2 M, pH 4.0), 0.1 mL of 50 μg $mL^{-1}$ Pd NPs/$CeO_2$ NTs, 0.1 mL of 5 mM TMB, 0.1 mL of 9.8 M $H_2O_2$, and 0.1 mL of the target solution were mixed together for reaction for 5 min, and then the UV–Vis spectra were measured.

## Results and discussion

### Characterization of Pd NPs/$CeO_2$ NTs

First, the synthesized materials were characterized by XRD. As shown in Figure S1 (Supporting Information), the XRD pattern of $CeO_2$ NTs prepared shows remarkable characteristic peaks. The intensive diffraction signals at $2\theta = 28.55°$, 33.08°, 47.48°, 56.34°, and 76.70° are corresponding to the (111), (200), (220), (311), and (331) planes of the cubic fluorite $CeO_2$ (JCPDS No. 43-1002), respectively. This result suggests the excellent crystallinity of $CeO_2$ NTs. With respect to the Pd NPs/$CeO_2$ NRs hybrid, as shown in Fig. 1a, the typical diffraction peaks of both Pd and $CeO_2$ are observed, while the peak intensity of $CeO_2$ decreases compared with that observed in the $CeO_2$ NTs material. This may be due to the coverage of the $CeO_2$ NRs surface by Pd NPs. In addition, the peaks of 40.16°, 46.62°, and 68.22° are assigned to the (111), (200), and (220) facets of the face-centered cubic structure of Pd (JCPDS No. 46-1043). These remarkable diffractions indicate the good crystallinity of the synthesized Pd NPs/$CeO_2$ NTs, and no other signal attributed to any impurity of Pd and Ce is found. The morphology of the as-prepared Pd NPs/$CeO_2$ NTs was investigated by TEM. According to the TEM image (Fig. 1b), a small number of Pd NPs seem not to be attached to $CeO_2$ NTs, while most of the formed Pd NPs are dispersed well on the surface of $CeO_2$ NTs. The followed experiments also indicate that these Pd NPs and $CeO_2$ NTs are interconnected each other to provide the synergistically enhanced peroxidase-like activity. This result demonstrates the successful synthesis of the Pd NPs/$CeO_2$ NTs hybrid. The structure of Pd NPs/$CeO_2$ NTs offers some advantages: On the one hand, the high dispersion of active Pd NPs provides a large surface area for catalysis and increases their utilization; on the other hand, the $CeO_2$ NTs support can effectively reduce the aggregation of these Pd NPs in comparison with unsupported Pd NPs.

### Synergistically enhanced peroxidase-like activity of Pd NPs/$CeO_2$ NTs

Next, the potential peroxidase-like properties of the synthesized Pd NPs/$CeO_2$ NTs were studied by employing TMB and $H_2O_2$ as substrates. As shown in Fig. 2a, when TMB, $H_2O_2$, and Pd NPs/$CeO_2$ NTs are mixed together, a rapid color change is observed, offering a maximum absorbance at approximately 652 nm. This color change should be attributed to the oxidation of colorless TMB into its blue product TMBox catalyzed by the Pd NPs/$CeO_2$ NTs hybrid in the presence of $H_2O_2$ [14, 15]. In the absence of TMB or $H_2O_2$, no obvious color reaction is observed. It should be stated that TMB can also be slowly oxidized by $H_2O_2$ in the absence of any catalyst under the same condition. As a result, a slight color change of the $H_2O_2$ + TMB system is also found. This phenomenon may be explained by the slow decomposition of the $H_2O_2$ substrate into hydroxyl radicals, which can further catalyze the oxidation of TMB.

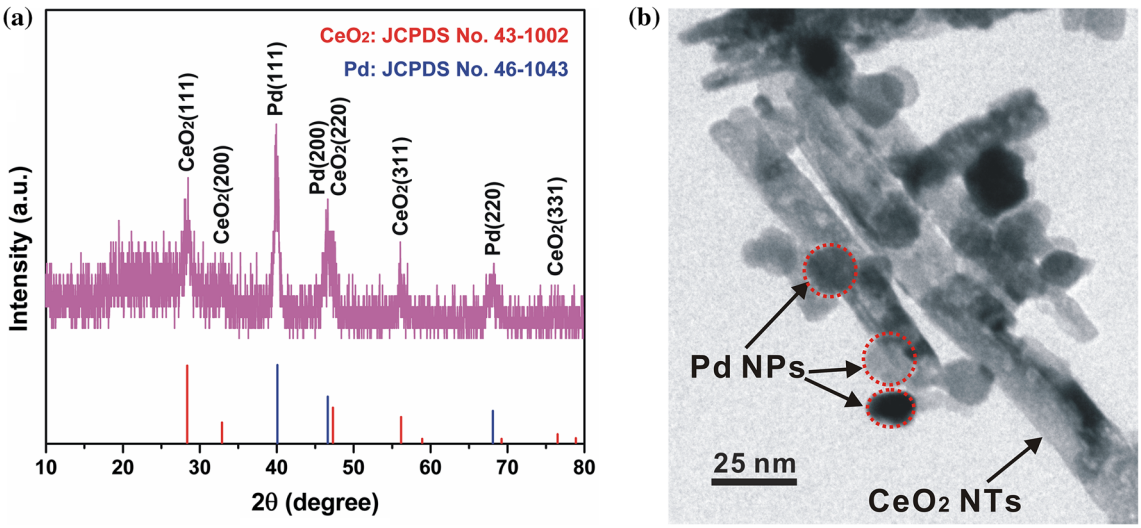


**Figure 1** **a** XRD pattern of the synthesized Pd NPs/$CeO_2$ NTs. **b** TEM image of the Pd NPs/$CeO_2$ NTs hybrid.

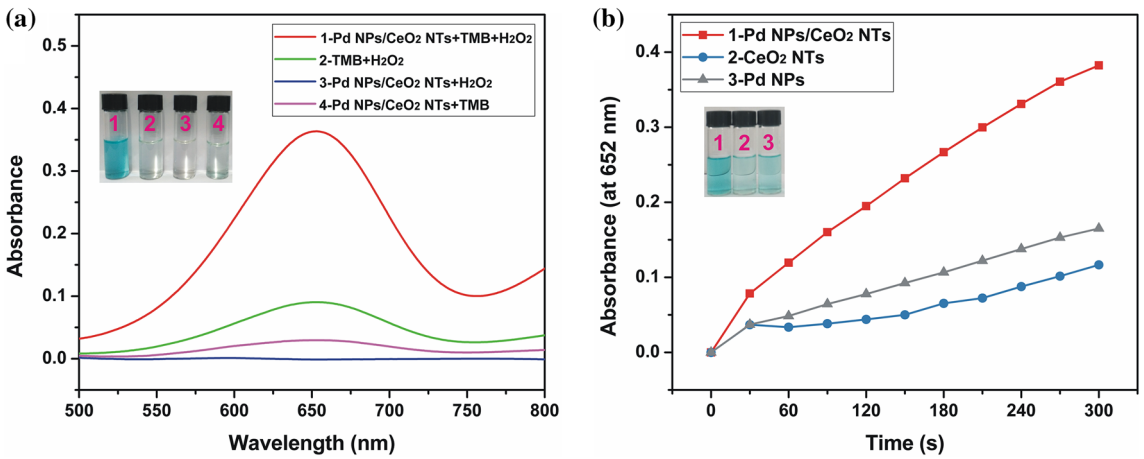


**Figure 2** **a** UV–Vis spectra of different systems, and the inset is the corresponding photograph. **b** Time-dependent absorbance changes of the TMB + $H_2O_2$ system catalyzed by different peroxidase mimics, and the inset is the corresponding photograph.

Taken together, the results shown in Fig. 2a demonstrate that the Pd NPs/$CeO_2$ NTs hybrid indeed induces the rapid oxidation of TMB mediated by $H_2O_2$, indicative of the peroxidase-like features of the synthesized Pd NPs/$CeO_2$ NTs. This finding is also verified by the time-dependent absorbance changes of the corresponding systems. As depicted in Figure S2 (Supporting Information), the Pd NPs/$CeO_2$ NTs peroxidase mimic triggers a fast increase in the absorbance at 652 nm upon reaction time, while in other systems no obvious change is obtained. In addition, the color reaction of the TMB + $H_2O_2$ system catalyzed by the Pd NPs/$CeO_2$ NTs nanozyme is influenced by several factors. As displayed in Figure S3 (Supporting Information), the absorbance increases along with the increasing concentrations of the peroxidase mimic. Similar to natural horseradish peroxidase (HRP), the peroxidase-like catalytic activity of the Pd NPs/$CeO_2$ NTs hybrid can be affected by buffer pH and reaction temperature. As presented in Figure S4(A) (Supporting Information), a volcano-type change of the nanozyme activity is found when the buffer pH increases from 2 to 7, with a maximum activity at pH 4. The reason for the absorbance decline at higher pH can be assigned to the inhibition of $H_2O_2$ decomposition when the buffer pH further increases [37]. The influence of reaction temperature on the mimetic activity of the hybrid is depicted in Figure S4(B) (Supporting Information). Similar to other peroxidase-mimicking nanozymes [34, 38, 39], the activity of the Pd NPs/$CeO_2$ NTs hybrid increases when the reaction temperature increases until to an optimal value, and then its activity measured drops when the reaction temperature further increases. It is interestingly found that the Pd NPs/$CeO_2$ NTs hybrid provides a maximum activity at 20 °C, which is a little lower than those observed in other nanozyme systems. The reason for this phenomenon is still unclear, and it needs further study.

In contrast to natural bio-enzymes, one of the most attractive merits of nanozymes is their stronger resistance against harsh environments. To check this feature in our synthesized nanozyme, the Pd NPs/$CeO_2$ NTs hybrid was first incubated in solutions with various pH values or at different temperatures for 2 h, and then its activity was measured under standard conditions. Our previous studies have revealed that natural HRP exhibits high activity only in neutral media [14–16]. With pH decreases or increases, its activity is sharply reduced, and no activity is found in strong acid solutions. With regard to temperature, the activity of HRP rapidly decreases when the incubation temperature exceeds 45 °C. In contrast, as depicted in Figure S5 (Supporting Information), the proposed Pd NPs/$CeO_2$ NTs exhibits no remarkable decline in activity when it is incubated in buffers with a wide range of pH or at different temperatures. These results confirm the excellent robustness of the peroxidase mimic.

More interestingly, the Pd NPs/$CeO_2$ NTs hybrid can exhibit a synergy effect in activity compared with individual Pd NPs and $CeO_2$ NTs. As verified in Fig. 2b, both Pd NPs and $CeO_2$ NTs are active to induce the color reaction of TMB in the presence of $H_2O_2$, providing the steady increase in the

absorbance at 652 nm upon reaction time. In comparison with the Pd NPs/$CeO_2$ NTs hybrid, the reaction rates observed in individual Pd NPs and $CeO_2$ NTs are much slower, which in return suggests the significantly improved activity of the synthesized Pd NPs/$CeO_2$ NTs.

To highlight the enhanced peroxidase-like activity of the Pd NPs/$CeO_2$ NTs hybrid, we carried out a series of control experiments. The enzymatic activities of $CeO_2$ NTs, Pd NPs, a simple mixture of $CeO_2$ NTs and Pd NPs (Pd NPs + $CeO_2$ NTs), and Pd NPs/$CeO_2$ NTs were measured. As compared in Fig. 3, the Pd NPs/$CeO_2$ NTs hybrid leads to the largest absorbance of the color reaction among these mimics, suggesting the highest peroxidase-like activity of the hybrid. What should be noted is that the Pd NPs/$CeO_2$ NTs hybrid can provide much improved activity in comparison with Pd NPs + $CeO_2$ NTs. This result indicates that the enhanced activity observed in the hybrid is not due to the simple mixing of Pd NPs and $CeO_2$ NTs, but originates from the interactions between the two entities. These control experiments also suggest that the attractive peroxidase-mimicking activity of Pd NPs/$CeO_2$ NTs mainly originates from the composite.

To quantitatively assess the catalytic activity of Pd NPs/$CeO_2$ NTs in contrast to those of individual

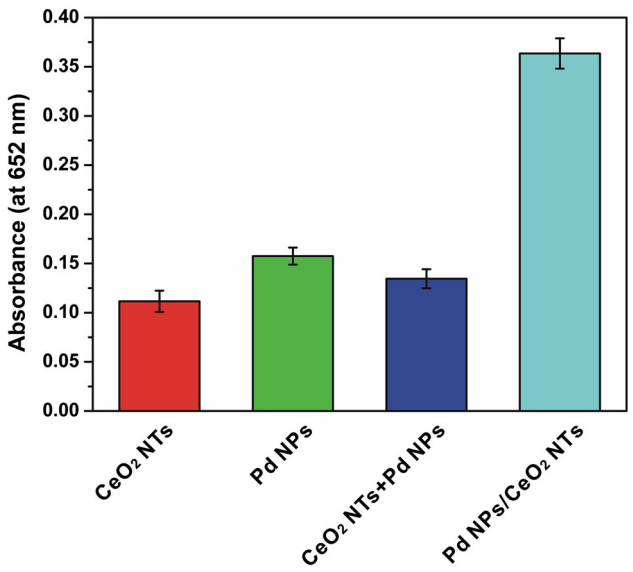


**Figure 3** Absorbance values of the TMB + $H_2O_2$ mixture catalyzed by different peroxidase mimics [the error bars represent the corresponding standard deviation (SD) of three parallel measurements].

$CeO_2$ NTs and Pd NPs, steady-state kinetic measurements for these peroxidase mimics were further carried out. As depicted in Figure S6 (Supporting Information), typical Michaelis–Menten curves are observed for all nanozymes toward the two substrates. The kinetic parameters are compared in Table 1. The $K_m$ values obtained in the Pd NPs/$CeO_2$ NTs hybrid are equal to those in Pd NPs, suggesting the comparative affinities of the two nanozymes to substrates. The $k_{cat}$ value of Pd NPs/$CeO_2$ NTs toward the $H_2O_2$ substrate is 2.3 and 3.8 times larger than that of $CeO_2$ NTs and Pd NPs, respectively. The $k_{cat}$ value of the former toward TMB is 1.3 and 3.9 times higher than that of the Pd NPs and $CeO_2$ NTs counterparts, respectively. The catalytic efficiency, defined by $k_{cat}/K_m$, is also the highest in the proposed hybrid. These data also demonstrate the Pd NPs/$CeO_2$ NTs hybrid as a desirable peroxidase mimic with improved activity and efficiency toward TMB and $H_2O_2$.

Afterward, the underlying reason why the synthesized hybrid can offer promoted enzymatic activity and efficiency compared with individual $CeO_2$ NTs and Pd NPs was explored. Previous works have verified that the interactions between noble meal and ceria in numerous noble metal–ceria composites have great influence on their catalytic activities [40–42]. In our work, it is also speculated that the enhanced activity observed in the Pd NPs/$CeO_2$ NTs hybrid may be related to the interplays between the Pd NPs and $CeO_2$ NTs entities. To verify this hypothesis, XPS was employed to probe the surface chemistry of the Pd NPs/$CeO_2$ NTs hybrid in comparison with individual $CeO_2$ NTs and Pd NPs. Figure 4a presents the high-resolution Ce 3d XPS pattern of the Pd NPs/$CeO_2$ NTs hybrid. The peaks at 898.43 and 917.08 eV correspond to $Ce^{IV}$ $3d_{5/2}$ and $Ce^{IV}$ $3d_{3/2}$, respectively. The signals at 883.21 and 901.33 eV are attributed to $Ce^{III}$ $3d_{5/2}$ and $Ce^{III}$ $3d_{3/2}$, respectively. Additional satellite lines $SU_1$, $SU_2$, and SD (SU and SD mean 'shake-up' and 'shake-down,' respectively [43, 44]) are shown at 902.93, 907.88, and 899.73 eV in the $Ce^{III}$ $3d_{3/2}$ part and at 885.03, 889.38, and 882.58 eV in the $Ce^{III}$ $3d_{5/2}$ part, respectively. In comparison with the $CeO_2$ NTs counterpart (Figure S7, Supporting Information), there is no significant change in peak positions, while the $Ce^{III}/Ce^{IV}$ ratio in the Pd NPs/$CeO_2$ NTs hybrid has a remarkable increase, as listed in Table 2. The increase in the $Ce^{III}/Ce^{IV}$ ratio should be attributed to the interactions between $CeO_2$ NTs and

**Table 1** Comparison of the kinetic parameters of Pd NPs/$CeO_2$ NTs, $CeO_2$ NTs, and Pd NPs toward $H_2O_2$ and TMB, respectively

| Nanozyme | Substrate | $K_m$ (mM) | $V_{max}$ ($\times 10^{-8}$ M $s^{-1}$) | [E] (μM) | $k_{cat}$ ($s^{-1}$) | $k_{cat}/K_m$ ($s^{-1}$ $M^{-1}$) |
|---|---|---|---|---|---|---|
| Pd NPs | $H_2O_2$ | 4.50 | 0.84 | 13 | $6.46 \times 10^{-4}$ | 0.14 |
| | TMB | 0.74 | 4.42 | 13 | $3.40 \times 10^{-3}$ | 4.59 |
| $CeO_2$ NTs | $H_2O_2$ | 28.63 | 0.50 | 13 | $3.85 \times 10^{-4}$ | 0.01 |
| | TMB | 0.45 | 1.54 | 13 | $1.18 \times 10^{-3}$ | 2.62 |
| Pd NPs/$CeO_2$ NTs | $H_2O_2$ | 9.43 | 1.91 | 13 | $1.47 \times 10^{-3}$ | 0.15 |
| | TMB | 0.39 | 5.94 | 13 | $4.57 \times 10^{-3}$ | 11.71 |

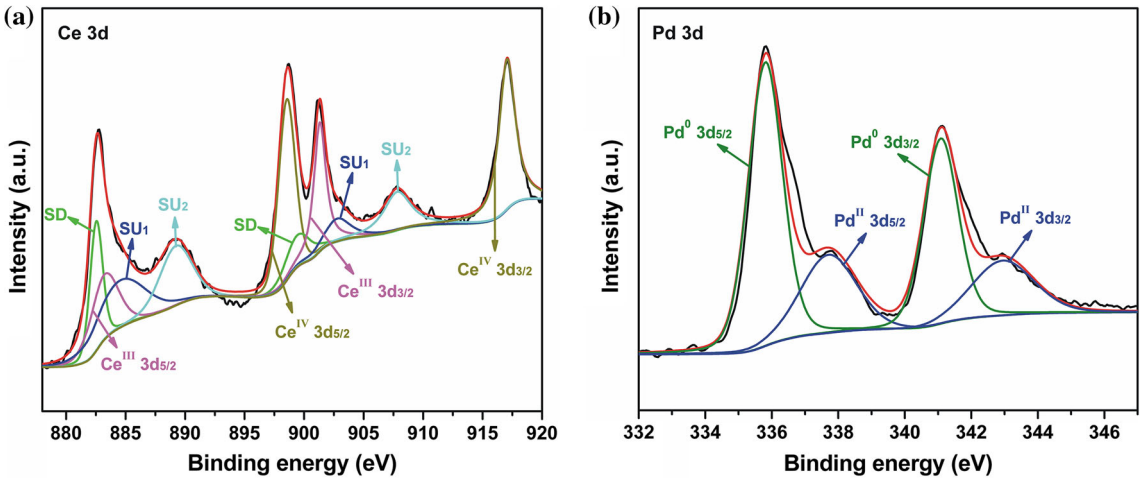


**Figure 4** **a** Ce 3d and **b** Pd 3d XPS patterns of the Pd NPs/$CeO_2$ NTs hybrid.

**Table 2** Comparison of the $Pd^0/Pd^{II}$ and $Ce^{III}/Ce^{IV}$ ratios in different nanozymes

| Nanozyme | $Pd^0/Pd^{II}$ | $Ce^{III}/Ce^{IV}$ |
|---|---|---|
| Pd NPs | 1.9 | – |
| $CeO_2$ NTs | – | 0.101 |
| Pd NPs/$CeO_2$ NTs | 2.1 | 0.358 |

Pd NPs. To be specific, Pd causes a change of the electronic states on the surface of $CeO_2$ NTs and thus contributes to a shorter distance between O and Pd. Consequently, the oxygen atom is readily reduced, and at the same time, $Ce^{IV}$ is easily transferred to the low oxidation state of $Ce^{III}$, thus resulting in the increase in the $Ce^{III}/Ce^{IV}$ ratio. This increase is closely related to the enhanced peroxidase-like activity of ceria-based nanozymes [30, 45]. Figure 4b presents the high-resolution Pd 3d XPS pattern of the Pd NPs/$CeO_2$ NTs hybrid. The peaks at 337.73 and 342.98 eV should be ascribed to $Pd^{II}$ $3d_{5/2}$ and $Pd^{II}$ $3d_{3/2}$, respectively. The peaks at 335.83 and 341.08 eV are attributed to $Pd^0$ $3d_{5/2}$ and $Pd^0$ $3d_{3/2}$, respectively. In comparison with the Pd NPs counterpart (Figure S8, Supporting Information), the $Pd^0/Pd^{II}$ ratio in Pd NPs/$CeO_2$ NTs has no obvious change (Table 2). To further uncover whether the enhanced activity of the hybrid originates from the reduced-state $CeO_2$ NTs or the interactions between Pd NPs and $CeO_2$ NTs, we evaluated the catalytic performance of $CeO_2$ NTs treated by $NaBH_4$ under the same condition. As shown in Figure S9 (Supporting Information), the absorbance observed in the reduced $CeO_2$ NTs is slightly higher than the untreated $CeO_2$ NTs, but still much lower than the Pd NPs/$CeO_2$ NTs hybrid. This comparison reveals that the enhanced activity observed should be attributed to the synergy effect of the two entities. In short, the interplays between the Pd NPs and $CeO_2$ NTs entities result in the significant increase in the $Ce^{III}/Ce^{IV}$ ratio, which further promotes the enzymatic activity and efficiency of the Pd NPs/$CeO_2$ NTs hybrid.

## Application of the Pd NPs/$CeO_2$ NTs nanozyme for sensing of sulfhydryl compounds

With no doubt, the peroxidase-like properties of the Pd NPs/$CeO_2$ NTs hybrid will endow them with extensive applications in various fields. With the enhanced activity, the hybrid can effectively catalyze the TMB + $H_2O_2$ reaction at a low concentration, which will reduce the amount of the two components used, especially the noble metal Pd. In this work, the excellent activity and robustness of the proposed Pd NPs/$CeO_2$ NTs peroxidase mimic inspire us to explore its potential application in biochemical analysis. Similar to other peroxidase-mimicking nanozymes [46–48], it is interestingly found that the color reaction of TMB + $H_2O_2$ catalyzed by Pd NPs/$CeO_2$ NTs is able to be suppressed by sulfhydryl compounds like mercaptoacetic acid. As demonstrated in Fig. 5a, the presence of mercaptoacetic acid leads to the decrease in the UV–Vis spectrum. In addition, the decreased absorbance highly depends on the level of mercaptoacetic acid added. This suppressed color reaction has also been confirmed by previous studies. According to the previous report [49], the SH-containing compounds (such as TGA) can suppress the $H_2O_2$ + TMB color reaction by competitively inhibiting the enzymatic activity of peroxidase mimics used. On the one hand, sulfhydryl compounds like mercaptoacetic acid are easy to be adsorbed onto the surface of Pd via the S–Pd bond [50], thus resulting in the coverage of the active sites in Pd; on the other hand, mercaptoacetic acid is more prone to be oxidized to form a disulfide, which can be verified by the lower redox potential of mercaptoacetic acid than TMB [51]. Therefore, the inhibited activity of the peroxidase mimic and/or the competitive reaction of sulfhydryl-containing species against TMB with generated hydroxyl radicals result in the suppressed color reaction, as illustrated in Fig. 5b. With this principle, mercaptoacetic acid in the concentration range of 66–400 nM is linearly detected (Figure S10, Supporting Information), and the linear equation is $Y = 0.26 - 4.86 \times 10^{-4}X$ ($R^2 = 0.958$). Based on the signal-to-noise ratio of three ($S/N = 3$) rule, the limit of detection (LOD) is calculated to be 45.3 nM.

To further demonstrate the practicability of our colorimetric method for detecting TGA, an environmental water sample collected was tested. As summarized in Table 3, the recoveries provided by the fabricated sensor are in the range of 130–145%. This means that the water sample contains some other substances that can also suppress the color reaction. Even so, the developed assay has great promise to be used for the semiquantitative detection of SH-containing targets.

Similarly, biothiols including cysteine and glutathione can also be determined with good performance. Figure 6a records the relationship between the absorbance at 652 nm and the concentration of cysteine and glutathione, respectively. The absorbance decreases along with the increasing concentrations of the two targets. Linear curves of the absorbance upon the Cys or GHS content in the scope range of 6–40 nM are observed (Fig. 6b), and the linear equations are $Y = 0.53 - 0.0083X$ ($R^2 = 0.985$) and $Y = 0.16 - 0.0023X$ ($R^2 = 0.977$), respectively.

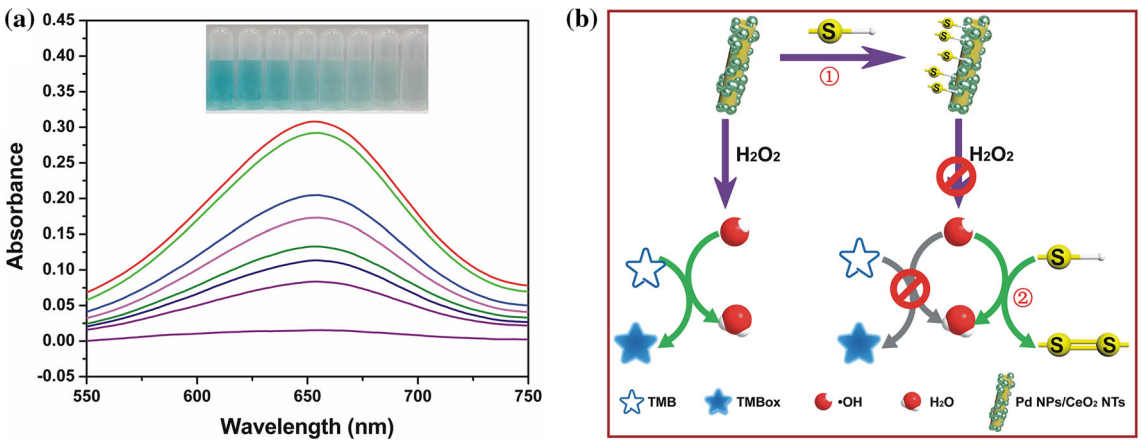


**Figure 5** **a** UV–Vis spectra of the TMB + $H_2O_2$ + Pd NPs/$CeO_2$ NTs system with the presence of mercaptoacetic acid at various concentrations, and the inset is the corresponding photograph. **b** Possible mechanism for the suppressed color reaction.

**Table 3** Recovery results for the detection of TGA in an environmental water sample

| Spiked (nM) | Detected (nM) | Recovery (%) |
|---|---|---|
| – | 104.0 ± 3.6 | – |
| 30 | 143.5 ± 4.0 | 131.7 |
| 60 | 183.2 ± 3.5 | 132.0 |
| 90 | 231.2 ± 4.7 | 141.3 |

The LOD values are further calculated to be 2.9 and 11.3 nM, respectively. Compared with previously reported methods for Cys or/and GHS sensing, as listed in Table 4, our assay is able to offer comparable performance in terms of LOD. More attractively, in comparison with electrochemical and fluorometric measurements, the target can be visually detected with naked eyes by using our sensor, and no other equipment is required. Thus, the sensor can be easily equipped with a smartphone for in-field analysis [52]. Different from most other sensors that provide linear responses for the targets at high concentrations (from sub-μM to μM levels), our sensor can be used to linearly detect the targets at the nM level. This phenomenon may be related to the unique Pd NPs/$CeO_2$ NTs mimic. Different from other peroxidase mimics like $Fe_3O_4$ MNPs, in our system sulfhydryl compounds can not only competitively react with generated hydroxyl radicals but also reduce the catalytic activity of the peroxidase mimic by adsorption on the surface of active Pd NPs via the Pd–S bond. The dual-functional effect of sulfhydryl compounds can significantly suppress the color reaction at a low concentration. These characteristics will endow it with great promise for the sensing of trace biothiols.

To check whether the thiol detection can be achieved without interferences using the Pd NPs/$CeO_2$ NTs hybrid, the selectivity was also

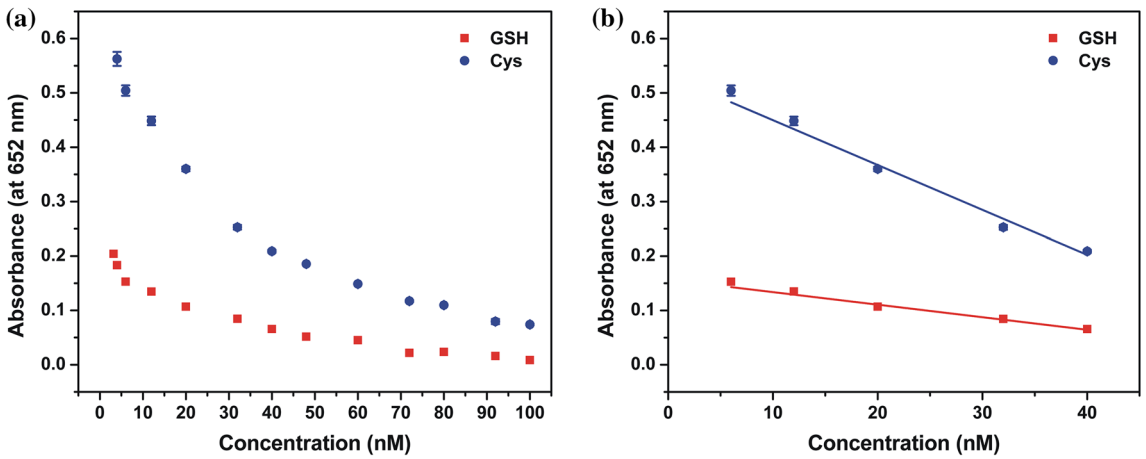


**Figure 6** **a** Relationship between the absorbance at 652 nm and the target (GSH or Cys) concentration. **b** Linear fitting of the absorbance and the target (GSH or Cys) level.

**Table 4** Comparison of Cys and GSH sensing performance of our assay with previously reported methods

| Material | Target | Method | Linear range | LOD | References |
|---|---|---|---|---|---|
| BCNT | Cys | Electrochemical | 0.78–200 μM | 0.26 μM | [53] |
| DNA-Au NPs | Cys | Colorimetric | 0.05–10 μM | 100 nM | [54] |
| MWCNT-AuNR | Cys | Electrochemical | 5–200 μM | 8.25 nM | [55] |
| MB/$Hg^{2+}$ | Cys | Fluorometric | 4–200 nM | 4.2 nM | [56] |
| | GSH | Fluorometric | 4–200 nM | 4.1 nM | |
| $Fe_3O_4$ MNPs | GSH | Colorimetric | 3–30 μM | – | [57] |
| CNFs | Cys | Electrochemical | 0.15–64 μM | 0.1 μM | [58] |
| PBI-$Hg^{2+}$ | Cys | Fluorometric | 0.05–0.3 μM | 9.6 nM | [59] |
| PMAA-$Ag^{+}$ | Cys | Fluorometric | 0.025–6.0 μM | 20 nM | [60] |
| Pd NPs/$CeO_2$ NTs | Cys | Colorimetric | 6–40 nM | 2.9 nM | Our work |
| | GSH | | 6–40 nM | 11.3 nM | |

investigated. As shown in Fig. 7, it is found that only Cys and GSH make a significant inhibition of the absorbance at 652 nm, while other nineteen amino acids, including sulfur-containing serine and methionine, provide no remarkable change in the absorbance. This result confirms that the Pd NPs/$CeO_2$ NTs hybrid can be used for the determination of biothiols selectively.

## Conclusions

In summary, we have proposed a Pd NPs/$CeO_2$ NTs peroxidase mimic that shows synergistically improved activity and efficiency for the colorimetric determination of sulfhydryl compounds. In comparison with individual Pd NPs and $CeO_2$ NTs, the strong interactions between the Pd NPs and $CeO_2$ NTs entities make the Pd NPs/$CeO_2$ NTs hybrid exhibit a synergy effect to trigger the color reaction of TMB in the presence of $H_2O_2$. Based on the suppression effect of sulfhydryl compounds toward the color reaction, sulfhydryl-containing species including mercaptoacetic acid, cysteine, and glutathione have been successfully detected with good performance. With the favorable enzymatic properties, the Pd NPs/$CeO_2$ NTs mimic will find great promise in other chemo- and biosensing applications.

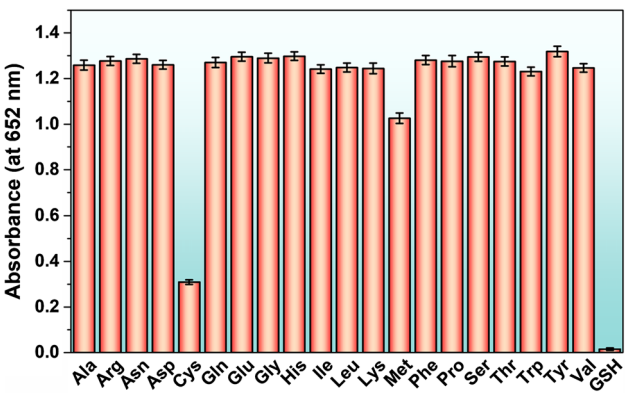


**Figure 7** Responses of the Pd NPs/$CeO_2$ NTs hybrid for the selective detection of biothiols against other amino acids. The concentrations of Cys, GSH, and other amino acid were kept at 100 μM.

## Acknowledgements

This work was carried out with the supports from the National Natural Science Foundation of China (Nos. 21605061 and 31601549), the Natural Science Foundation of Jiangsu Province (No. BK20160489), the Natural Science Fund for Colleges and Universities in Jiangsu Province (No. 16KJB150009), the Postdoctoral Fund of China (No. 2016M600365), the Postdoctoral Fund of Jiangsu Province (No. 1601015B), the Open Fund from the Shanghai Key Laboratory of Functional Materials Chemistry (No. SKLFMC201601), the Open Fund from the State Key Laboratory of Bioreactor Engineering, and the Cultivation Project for Excellent Young Teachers in Jiangsu University.

**Electronic supplementary material:** The online version of this article (https://doi.org/10.1007/s10853-018-2657-x) contains supplementary material, which is available to authorized users.

## References

[1] Wei H, Wang EK (2013) Nanomaterials with enzyme-like characterics (nanozymes): next-generation artificial enzymes. Chem Soc Rev 42:6060–6093

[2] Gao LZ, Yan XY (2013) Discovery and current application of nanozyme. Progress Biochem Biophys 40:892–902

[3] Wang XY, Guo WJ, Hu YH, Wu JJX, Wei H (2016) Nanozymes: next wave of artificial enzymes. Springer, New York

[4] Gao LZ, Fan KL, Yan XY (2017) Iron oxide nanozyme: a multifunctional enzyme mimetic for biomedical applications. Theranostics 7:3207–3227

[5] Ragg R, Tahir MN, Tremel W (2016) Solids go bio: inorganic nanoparticles as enzyme mimics. Eur J Inorg Chem 2016:1906–1915

[6] Lin YH, Ren JS, Qu XG (2014) Catalytically active nanomaterials: a promising candidate for artificial enzymes. Acc Chem Res 47:1097–1105

[7] Wang XY, Hu YH, Wei H (2016) Nanozymes in bionanotechnology: from sensing to therapeutics and beyond. Inorg Chem Front 3:41–60

[8] Li W, Chen B, Zhang HX, Sun YH, Wang J, Zhang JL, Fu Y (2015) BSA-stabilized Pt nanozyme for peroxidase mimetics and its application on colorimetric detection of mercury(II) ions. Biosens Bioelectron 66:251–258

[9] Wang K, Fan DQ, Liu YQ, Wang EK (2015) Highly sensitive and specific colorimetric detection of cancer cells via

dual-aptamer target binding strategy. Biosens Bioelectron 73:1–6

[10] Cui ML, Zhao Y, Wang C, Song QJ (2017) The oxidase-like activity of iridium nanoparticles, and their application to colorimetric determination of dissolved oxygen. Microchim Acta 184:3113–3119

[11] Ding N, Yan N, Ren CL, Chen XG (2010) Colorimetric determination of melamine in dairy products by $Fe_3O_4$ magnetic nanoparticles-$H_2O_2$-ABTS detection system. Anal Chem 82:5897–5899

[12] Liang MM, Fan KL, Pan Y et al (2013) $Fe_3O_4$ magnetic nanoparticle peroxidase mimetic-based colorimetric assay for the rapid detection of organophosphorus pesticide and nerve agent. Anal Chem 85:308–312

[13] Wei H, Wang EK (2008) $Fe_3O_4$ magnetic nanoparticles as peroxidase mimetics and their applications in $H_2O_2$ and glucose detection. Anal Chem 80:2250–2254

[14] He YF, Niu XH, Shi LB et al (2017) Photometric determination of free cholesterol via cholesterol oxidase and carbon nanotube supported Prussian blue as a peroxidase mimic. Microchim Acta 184:2181–2189

[15] Niu XH, He YF, Pan JM et al (2016) Uncapped nanobranch-based CuS clews used as an efficient peroxidase mimic enable the visual detection of hydrogen peroxide and glucose with fast response. Anal Chim Acta 947:42–49

[16] Niu XH, He YF, Zhang WC, Li X, Qiu FX, Pan JM (2018) Elimination of background color interference by immobilizing Prussian blue on carbon cloth: a monolithic peroxidase mimic for on-demand photometric sensing. Sens Actuators, B 256:151–159

[17] Mumtaz S, Wang LS, Hussain SZ et al (2017) Dopamine coated $Fe_3O_4$ nanoparticles as enzyme mimics for the sensitive detection of bacteria. Chem Commun 53:12306–12308

[18] Yang ZJ, Cao Y, Li J, Lu MM, Jiang ZK, Hu XY (2016) Smart CuS nanoparticles as peroxidase mimetics for the design of novel label-free chemiluminescent immunoassay. ACS Appl Mater Interfaces 8:12031–12038

[19] Hu YH, Cheng HJ, Zhao XZ et al (2017) Surface-enhanced raman scattering active gold nanoparticles with enzyme-mimicking activities for measuring glucose and lactate in living tissues. ACS Nano 11:5558–5566

[20] Fu Y, Zhang HX, Dai SD, Zhi X, Zhang JL, Li W (2015) Glutathione-stabilized palladium nanozyme for colorimetric assay of silver(I) ions. Analyst 140:6676–6683

[21] Cai R, Yang D, Chen XG et al (2016) Three dimensional multipod superstructures based on $Cu(OH)_2$ as a highly efficient nanozyme. J Mater Chem B 4:4657–4661

[22] Tian R, Sun JH, Qi YF, Zhang BY, Guo SL, Zhao MM (2017) Influence of $VO_2$ nanoparticle morphology on the colorimetric assay of $H_2O_2$ and glucose. Nanomaterials 7:347

[23] Peng FF, Zhang Y, Gu N (2008) Size-dependent peroxidase-like catalytic activity of $Fe_3O_4$ nanoparticles. Chin Chem Lett 19:730–733

[24] He WW, Wu XC, Liu JB, Hu XN, Zhang K, Hou S, Zhou WY, Xie SS (2010) Design of AgM bimetallic alloy nanostructures (M = Au, Pd, Pt) with tunable morphology and peroxidase-like activity. Chem Mater 22:2988–2994

[25] Ghosh S, Roy P, Karmodak N, Jemmis ED, Mugesh G (2018) Nanoisozymes: crystal-facet-dependent enzyme-mimetic activity of $V_2O_5$ nanomaterials. Angew Chem Int Ed. https://doi.org/10.1002/ange.201800681

[26] Liu BW, Liu JW (2017) Surface modification of nanozymes. Nano Res 10:1125–1148

[27] Niu XH, He YF, Li X, Song HW, Zhang WC, Peng YX, Pan JM, Qiu FX (2017) Trace iodide dramatically accelerates the peroxidase activity of $VO_x$ at ppb-concentration levels. ChemistrySelect 2:10854–10859

[28] Wang QQ, Zhang XP, Huang L, Zhang ZQ, Dong SJ (2017) One-pot synthesis of $Fe_3O_4$ nanoparticle loaded 3D porous graphene nanocomposites with enhanced nanozyme activity for glucose detection. ACS Appl Mater Interfaces 9:7465–7471

[29] Zhang ST, Li H, Wang ZY, Liu J, Zhang HL, Wang BD, Yang ZY (2015) Strongly coupled Au/$Fe_3O_4$/GO hybrid material with enhanced nanozyme activity for highly sensitively colorimetric detection, rapid and efficient removal of $Hg^{2+}$ in aqueous solutions. Nanoscale 7:8495–8502

[30] Zhao H, Dong YM, Jiang PP, Wang GL, Zhang JJ (2015) Highly dispersed $CeO_2$ on $TiO_2$ nanotube: a synergistic nanocomposite with superior peroxidase-like activity. ACS Appl Mater Interfaces 7:6451–6461

[31] Wang N, Sun JC, Chen LJ, Fan H, Ai SY (2015) A $Cu_2(OH)_3Cl$–$CeO_2$ nanocomposite with peroxidase-like activity, and its application to the determination of hydrogen peroxide, glucose and cholesterol. Microchim Acta 182:1733–1738

[32] Artiglia L, Agnoli S, Paganini MC, Cattelan M, Granozzi G (2014) $TiO_2$@$CeO_x$ core–shell nanoparticles as artificial enzymes with peroxidase-like activity. ACS Appl Mater Interfaces 6:20130–20136

[33] Tao Y, Lin YH, Huang ZZ, Ren JS, Qu XG (2013) Incorporating graphene oxide and gold nanoclusters: a synergistic catalyst with surprisingly high peroxidase-like activity over a broad pH range and its application for cancer cell detection. Adv Mater 25:2594–2599

[34] Singh S, Tripathi P, Kumar N, Nara S (2017) Colorimetric sensing of malathion using palladium-gold bimetallic nanozyme. Biosens Bioelectron 92:280–286

[35] Lin YH, Xu C, Ren JS, Qu XG (2012) Using thermally regenerable cerium oxide nanoparticles in biocomputing to

perform label-free, resettable, and colorimetric logic operations. Angew Chem Int Ed 51:12579–12583

[36] Liu BW, Sun ZY, Huang JJ, Liu JW (2015) Hydrogen peroxide displacing DNA from nanoceria: mechanism and detection of glucose in serum. J Am Chem Soc 137:1290–1295

[37] Han L, Li CC, Zhang T, Lang QL, Liu AH (2015) Au@Ag heterogeneous nanorods as nanozyme interfaces with peroxidase-like activity and their application for one-pot analysis of glucose at nearly neutral pH. ACS Appl Mater Interfaces 7:14463–14470

[38] Xia XH, Zhang JT, Lu N, Kim MJ, Ghale KG, Xu Y, McKenzie E, Liu JB, Ye HH (2015) Pd–Ir core–shell nanocubes: a type of highly efficient and versatile peroxidase mimic. ACS Nano 9:9994–10004

[39] Ma JS, Wang Y, Zhao M, Zhang L (2012) Intrinsic peroxidase-like activity and catalase-like activity of $Co_3O_4$ nanoparticles. Chem Commun 48:2540–2542

[40] Bera P, Patil KC, Jayaram V, Subbanna GN, Hegde MS (2000) Ionic dispersion of Pt and Pd on $CeO_2$ by combustion method: effect of metal-ceria interaction on catalytic activities for NO reduction and CO and hydrocarbon oxidation. J Catal 196:293–301

[41] Bruix A, Rodriguez JA, Ramírez PJ et al (2012) A new type of strong metal-support interaction and the production of $H_2$ through the transformation of water on Pt/$CeO_2$(111) and Pt/$CeO_x$/$TiO_2$(110) catalysts. J Am Chem Soc 134:8968–8974

[42] Li ZH, Yang XD, Yang YB, Tan YN, He Y, Liu M, Liu XW, Yuan Q (2018) Peroxidase-mimicking nanozyme with enhanced activity and high stability based on metal-support interactions. Chem Eur J 24:409–415

[43] Tsunekawa S, Fukuda T, Kasuya A (2000) X-ray photoelectron spectroscopy of monodisperse $CeO_{2-x}$ nanoparticles. Surf Sci 457:L437–L440

[44] Vercaemst R, Poelman D, Meirhaeghe RLV, Fiermans L, Laflère WH, Cardon F (1995) An XPS study of the dopants'valence states and the composition of CaS1–*x*Sex: Eu and SrS1–*x*Sex: Ce thin film electroluminescent devices. J Lumin 63:19–30

[45] Tian ZM, Li J, Zhang ZY, Gao W, Zhou XM, Qu YQ (2015) Highly sensitive and robust peroxidase-like activity of porous nanorods of ceria and their application for breast cancer detection. Biomaterials 59:116–124

[46] Fu Y, Zhao XY, Zhang JL, Li W (2014) DNA-based platinum nanozymes for peroxidase mimetics. J Phys Chem C 108:18116–18125

[47] Li SQ, Wang LT, Zhang XD, Chai HX, Huang YM (2018) A Co, N co-doped hierarchically porous carbon hybrid as a highly efficient oxidase mimetic for glutathione detection. Sens Actuators, B 264:312–319

[48] Feng JY, Huang PC, Shi SZ, Deng KY, Wu FY (2017) Colorimetric detection of glutathione in cells based on peroxidase-like activity of gold nanoclusters: a promising powerful tool for identifying cancer cells. Anal Chim Acta 967:64–69

[49] Singh M, Weerathunge P, Liyanage PD, Mayes E, Ramanathan R, Bansal V (2017) Competitive inhibition of the enzyme-mimic activity of Gd-based nanorods toward highly specific colorimetric sensing of L-cysteine. Langmuir 33:10006–10015

[50] Webb JD, Quarrie SM, Eleney KM, Crudden CM (2007) Mesoporous silica-supported Pd catalysts: an investigation into structure, activity, leaching and heterogeneity. J Catal 252:97–109

[51] Roy A, Sahoo R, Ray C, Dutta S, Pal T (2016) Soft template induced phase selective synthesis of $Fe_2O_3$ nanomagnets: one step towards peroxidase-mimic activity allowing colorimetric sensing of thioglycolic acid. RSC Adv 6:32308–32318

[52] Cheng N, Song Y, Zeinhom MMA, Chang YC, Sheng L, Li HL (2017) Nanozyme-mediated dual immunoassay integrated with smartphone for use in simultaneous detection of pathogens. ACS Appl Mater Interfaces 9:40671–40680

[53] Deng CY, Chen JH, Chen XL, Wang MD, Nie Z, Yao SZ (2009) Electrochemical detection of L-cysteine using a boron-doped carbon nanotube-modified electrode. Electrochim Acta 54:3298–3302

[54] Lee JS, Ulmann PA, Han MS, Mirkin CA (2007) A DNA-gold nanoparticle-based colorimetric competition assay for the detection of cysteine. Nano Lett 8:529–533

[55] Silva FAS, Silva MGA, Lima PR, Meneghetti MR, Kubota LT, Goulart MOF (2013) A very low potential electrochemical detection of L-cysteine based on a glassy carbon electrode modified with multi-walled carbon nanotubes/gold nanorods. Biosens Bioelectron 50:202–209

[56] Xu H, Hepel M (2011) "Molecular beacon"-based fluorescent assay for selective detection of glutathione and cysteine. Anal Chem 83:813–819

[57] Ma YH, Zhang ZY, Ren CL, Liu GY, Chen XG (2012) A novel colorimetric determination of reduced glutathione in A549 cells based on $Fe_3O_4$ magnetic nanoparticles as peroxidase mimetics. Analyst 137:485–948

[58] Tang XF, Liu Y, Hou HQ, You TY (2010) Electrochemical determination of L-tryptophan, L-tyrosine and L-cysteine using electrospun carbon nanofibers modified electrode. Talanta 80:2182–2186

[59] Ruan YB, Li AF, Zhao JS, Shen JS, Jiang YB (2010) Specific $Hg^{2+}$-mediated perylene bisimide aggregation for highly sensitive detection of cysteine. Chem Commun 46:4938–4940

[60] Shang L, Dong SJ (2009) Sensitive detection of cysteine based on fluorescent silver clusters. Biosens Bioelectron 24:1569–1573